Boundary-Layer Meteorol (2011) 140:343–360
DOI 10.1007/s10546-011-9616-2

ARTICLE

The Near-Calm Stable Boundary Layer

Larry Mahrt

Received: 29 November 2010 / Accepted: 12 April 2011 / Published online: 13 May 2011

Abstract For the near-calm stable boundary layer, nominally 2-m mean wind speed $<0.5\,\mathrm{m\,s^{-1}}$, the time-average turbulent flux is dominated by infrequent mixing events. These events are related to accelerations associated with wave-like motions and other more complex small-scale motions. In this regime, the relationship between the fluxes and the weak mean flow breaks down. Such near-calm conditions are common at some sites. For very weak winds and strong stratification, the characteristics of the fluctuating quantities change slowly with increasing scale and the separation between the turbulence and non-turbulent motions can become ambiguous. Therefore, a new analysis strategy is developed based on the scale dependence of selected flow characteristics, such as the ratio of the fluctuating potential energy to the kinetic energy. In contrast to more developed turbulence, correlations between fluctuating quantities are small, and a significant heat flux is sometimes carried by very weak vertical motions with large temperature fluctuations. The relation of the flux events to small-scale increases of wind speed is examined. Large remaining uncertainties are noted.

Keywords Cold pool · Intermittency · Mixing events · Nocturnal boundary layer · Stable boundary layer

1 Introduction

In ‘near-calm’ thin stable boundary layers, turbulence is generated primarily by wave-like motions, microfronts and other more complex motions on time scales of minutes or tens of minutes. Based on our datasets, these conditions are common during cloudless synoptically inactive periods over flat terrain, and common for a wider range of conditions in valleys and basins where cold pools form (Heywood 1933; Whiteman 2000; Cuxart et al. 2007; Vosper and Brown 2008; Yao and Zhong 2009; Bodine et al. 2009; Mahrt et al. 2010). Near-calm conditions can be associated with the very poor dispersion of contaminants, low surface

L. Mahrt (✉)
Oregon State University, Corvallis, OR, USA
e-mail: mahrt@nwra.com

temperatures and/or the formation of dense fog. Although near-calm conditions are most common in very stable conditions, they also occur in neutral and unstable conditions.

The near-calm regime over relatively flat terrain is related to the 'radiation' case of Van de Wiel et al. (2003); the extremely weak turbulence case of Mahrt and Vickers (2006), stability class 5 from Basu et al. (2006) and the extremely stable conditions of Sorbjan (2010). For such conditions during the polar night, Grachev et al. (2005) found that Ekman rotation of the wind vector may become important even close to the surface, invalidating Monin–Obukhov similarity theory. Because of non-stationary shear generation of turbulence, the turbulence never completely vanishes and the concept of a critical Richardson number, above which the flow becomes laminar, does not apply (Zilitinkevich et al. 2007; Galperin and Sukoriansky 2010). Although the near-calm regime has received little modelling attention, the modelling analysis of Derbyshire (1999) provides insight into potential difficulties. Several features of the near-calm regime can be anticipated from studies in the literature:

1. The surface friction velocity (u_*) associated with the mean flow may no longer be a dominant governing velocity scale (Grachev et al. 2005; Sorbjan 2010). In such conditions, the Ekman number may become less than one, leading to significant rotation of the wind vector with height (Grachev et al. 2005). The non-dimensional shear, ϕ_m, may still be highly correlated to z/L because percentage-wise large erratic variations of u_* may dominate the variation of both ϕ_m and z/L, corresponding to self-correlation (Hicks 1981; Klipp and Mahrt 2003; Baas et al. 2006), where L is the Obukhov length.
2. Wind profiles often deviate substantially from normal boundary-layer structure described by similarity theory. Such profiles may include a near-surface wind maximum at heights as low as a few metres, inflection points and significant directional shear of either sign (Mahrt 2008). Near-surface wind maxima occur over flat terrain, but are particularly common in the presence of thin drainage flows. The directions of the mean wind, wind shear and stress vectors can deviate significantly in near-calm flow.
3. The 'boundary layer' may be sufficiently thin (Smedman 1988) that standard observational levels, even as low as 2 m, may be above the surface layer, if it exists.
4. Gravity waves with periods much larger than the largest turbulent time scales can lead to modulation of the turbulence as a result of clear separation between turbulence and wave scales (Finnigan et al. 1984; Sun et al. 2004; Meillier et al. 2008; Nappo et al. 2008; Tjernström et al. 2009; Fritts et al. 2009; Viana et al. 2009, 2010; Bou-Zeid et al. 2010). However, partitioning the fluctuations between turbulence, the smallest waves and other non-turbulent motions may be problematic for some situations, suggesting that these phenomena should be studied in concert (Galperin et al. 2007). There is no well-defined cut-off scale that separates the turbulence and non-turbulent motions; the motion characteristics vary continually with scale. The forcing of the turbulence itself becomes stochastic.
5. Forcing of turbulence by wave-like motions that are deep and/or propagate from distant sources may preclude local boundary-layer scaling (Finnigan 1999).
6. Time-averaged turbulence quantities may be strongly influenced by infrequent events (Howell and Sun 1999; Yagüe et al. 2006). The observed mixing events can be generated at the surface or result from downward bursting of turbulence (Nappo and Chimonas 1992). The nature of these transient events are site dependent (Mahrt 2009) and preclude simple universal theories. The mixing events in near-calm flow are less frequent than in most intermittency studies in the literature (Katul et al. 1994), yet can still dominate the

averaged fluxes. The mixing events appear to be often initiated by transient disturbances that are not captured in models (Belušić and Güttler 2010).

Near-calm cases have been often eliminated from existing analysis by imposed minimum conditions on turbulence intensity or non-stationarity, or they are simply eliminated as outliers. Since the physical understanding is too limited to form scaling variables, initial work must concentrate on basic understanding without scaling. Although the near-calm boundary layer is complex and will not yield to simple similarity theory, the current study reveals new information on characteristics of these seldom studied motions.

2 Data

The primary dataset is FLOSSII (Fluxes Over Snow-covered Surfaces II) collected from 1 December 2002 to 31 March 2003 in the North Park Basin of north-west Colorado, U.S.A. (Mahrt and Vickers 2006). While near-calm conditions occur more often for some of our other datasets, adequate vertical information is not available. The standard CASES-99 data set contains only two nights approaching our near-calm criteria and is not used here.

We have examined both tilt-rotated (Acevedo and Mahrt 2010) and unrotated data. The tilt correction does not significantly affect the turbulent heat fluxes, but can affect the turbulent momentum flux in weak-wind conditions depending on the tilt rotation method. It is not known if the tilt rotation leads to improved fluxes since the true flux is not known and the mean vertical motion may include a real directionally dependent contribution in very stable conditions where minor surface obstacles can significantly perturb the flow. This study uses unrotated data with the concession that momentum fluxes may be significantly influenced by sonic misalignment.

Automated quality control procedures may be too aggressive for very weak turbulence, particularly with those procedures that eliminate data with large kurtosis or skewness or very small u_*. Here, we eliminate only data where values exceed meteorologically impossible thresholds. 5-s and 1-min periods are eliminated when more than 30% of the data are missing. In addition, all records were visually checked for erratic behaviour, which was sometimes related to the icing of transducers.

Since the wind direction is constantly shifting in near-calm conditions, we cannot eliminate flow through the tower without fragmenting the time series. For very stable conditions, flux loss due to pathlength averaging may be significant and cospectral 'corrections' are of uncertain validity. The cospectra for the FLOSSII observations suggest that flux loss occurs primarily at the 1-m level where non-negligible fluxes occurred at the smallest resolved scales. The flux loss for the 2-m data analyzed in this study appears to be small.

Vertical temperature differences are estimated in terms of sonic anemometer temperatures, which were calibrated against aspirate thermistors (Mahrt 2007) during periods when they worked properly. The calibrated sonic anemometer temperatures were then checked for well-mixed conditions during cloudy strong-wind cases. Based on these comparisons, the error in the estimated vertical temperature difference could be 0.1–0.3 K. These errors are problematic for near-neutral conditions, but of little consequence for the cases of strong stratification.

3 Averaging Times

Turbulent fluxes are normally computed from deviations from an average computed over averaging time, τ_s. Choice of τ_s might be based on the cospectra or integrated cospectra,

as in the OGIVE approach (Desjardins et al. 1989; Friehe et al. 1991). Unfortunately, the separation of turbulence from non-turbulent motions becomes ambiguous in some near-calm conditions. This is due to a mix of turbulent and non-turbulent motions on a given time scale, including trends due to larger-scale non-turbulent motions. In addition, the characteristics of the motions dominating the flux only gradually change with increasing time scale. Instead of attempting to isolate the turbulence for near-calm conditions, we study the dependence of the flow characteristics on scale by crudely dividing the flow into three ranges of time scales:

(1) The most turbulent-like motions for near-calm winds extend up to time scales of about 5 s (Sect. 5). We loosely refer to fluctuations on time scales less than 5 s as 'turbulence' although even these short time scales include non-turbulent motions.
(2) We also analyze characteristics of deviations of 5-s averages from 1-min averages representing motions on time scales from 5 to 60 s. Motions on such scales for near-calm conditions do not generally satisfy classical turbulence expectations (Sect. 5), but in the mean, transport heat downward. These motions are characterized by large temperature fluctuations and weak vertical motions compared to the 0–5 s turbulence.
(3) Motions on time scales between 1 min and 1 h are dominated by wave-like modes, microfronts and frequently occurring more complex structures. These scales are characterized by erratic variation of fluxes, although Acevedo and Mahrt (2010) found a greater vertical coherence of such fluxes with specific choices of the sonic tilt rotation. The flux by motions on time scales of 1 min or more will not be considered further in this study.

Decomposing the flow into finer ranges of time scales, such as afforded by the wavelet decomposition, leads to better time-scale resolution. Within large scatter, this type of analysis shows continual variation of flow characteristics with increasing time scale. The broader ranges of time scales used in this study provide better sampling.

Turbulent fluxes are often averaged over a longer time scale, τ_F, to reduce sampling problems. This is particularly necessary in near-calm conditions where occasional events can dominate the flux. The chance occurrence of a single event can account for much of the total flux for a given hour. As a result, we choose a large value of τ_F, here equal to 6 h, beginning at 2300 local standard time and ending at 0500 local standard time. This provides one long record for each night. Averaging times longer than 6 h begin to incorporate more significant non-stationarity due to diurnal variation and synoptic scale variations. The standard error of the flux is small for almost all of the 6-h periods because of the long record length. However, the standard error is a poor measure of the uncertainty with near-calm conditions due to the large kurtosis and strong contribution of a limited number of events. For this reason, error bars are avoided in this study and scatter plots are sometimes used to indicate variability.

Six-hour periods are eliminated when more than 30% of the data are missing. Three of the remaining 133 6-h periods are characterized by very weak upward heat flux. We retain these records; if such an upward heat flux is due to random-like variation, eliminating these records would create a bias. Fluxes associated with the 0–5 and 5–60 s range of time scales will be averaged over 1 min for the analysis in Sect. 6, and averaged over 6 h for the analysis in the next section.

The 2-m vector-averaged wind speed over 6 h is bimodal with a relative maximum at about $4\,\mathrm{m\,s^{-1}}$, usually corresponding to synoptically active periods, and a second maximum

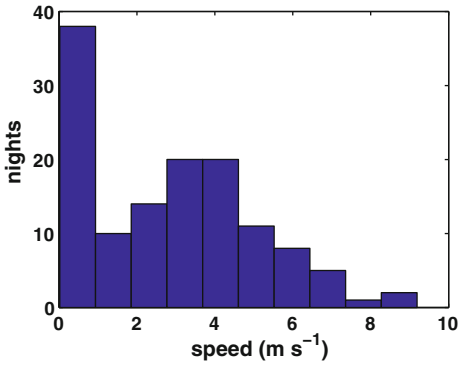

Fig. 1 Frequency distribution of the speed ($\mathrm{m\,s^{-1}}$) of the 6-h vector-averaged wind for the nocturnal period of 2300–0500 local standard time

for weak winds less than $1\,\mathrm{m\,s^{-1}}$ (Fig. 1). About 30% of the nocturnal records have a vector-averaged speed of less than $1\,\mathrm{m\,s^{-1}}$, and almost 25% of the total records have an averaged speed of less than $0.5\,\mathrm{m\,s^{-1}}$.

4 Quantifying Flow Characteristics

Existing analysis strategies, such as spectra and scaled quantities, are not effective in near-calm conditions. We now define quantities for describing the mean flow and the turbulence to contrast the near-calm regime with more significant winds using the entire nocturnal data set (133 6-h records).

4.1 Velocity Scales and Stability

Our general approach is to relate the turbulence exclusively to the mean flow and not to relate non-dimensional turbulence quantities to other non-dimensional turbulence quantities, as is common in similarity theory. For example, z/L will be used as a characteristic of the turbulence rather than a predictive stability parameter. We begin by reviewing the basic velocity scales that represent the mean flow. The speed of the 6-h vector-averaged wind

$$V \equiv ([u]^2 + [v]^2)^{0.5} \tag{1}$$

is evaluated at 2 m, the same level for evaluation of the turbulence quantities.

The mean shear

$$\delta V \equiv (([u(z_2)] - [u(z_1)])^2 + ([v(z_2)] - [v(z_1)])^2)^{0.5} \tag{2}$$

is evaluated between $z_1 = 1$ m and $z_2 = 10\,\mathrm{m}$. We define a buoyancy velocity as

$$V_\mathrm{b} \equiv \left(\frac{g\ \delta z\ \delta\theta}{\Theta}\right)^{0.5} \tag{3}$$

where $\delta\theta$ is the difference in potential temperatures between 1 and 10 m. Using temperatures over thinner layers leads to larger (percentage-wise) errors.

The sensitivity of the Richardson number to choice of levels and layer thickness, demonstrated in Balsley et al. (2008) and Tjernström et al. (2009), can become extreme for near-calm winds. The utility of the Richardson numbers suffers from extremely large values for near-calm cases. We instead define a version of the Froude number:

$$Fr \equiv \frac{V}{V_b} \tag{4}$$

where again V is the speed of the vector-averaged wind. Here, Fr is equivalent to the square root of the inverse of a bulk Richardson number.

For near-calm conditions, the turbulence is generated mainly by wave-like and other submeso motions and the turbulence becomes poorly related to the above mean velocity scales. 'Submeso' sometimes refers to the wide variety of motions on scales larger than the turbulence, but smaller than the minimum meso-γ scale (2 km). Here, we define a submeso velocity scale as

$$V_{sm} \equiv [\hat{u}^2 + \hat{v}^2]^{0.5} \tag{5}$$

where $\hat{\phi}$ is the deviation of the 1-min average from the 1-h average where ϕ is any variable, and again [ ] represents averaging over the 6-h record. The above velocity scale represents the kinetic energy of the submeso motions, and is not systematically related to the 6-h vector-averaged speed (not shown). The submeso activity is always present, but exerts a significant influence on the flow only when the mean wind speed is small. The relationship of the turbulence to the 1-min averaged flow is complex partly because the turbulence may not reach equilibrium with the constantly changing 1-min flow. Initial attempts to relate the turbulence to different scales contributing to V_{sm} failed to identify a dominant time scale.

We also define a generalized velocity scale as

$$V_{gen} \equiv \left(V^2 + \beta V_{sm}^2\right)^{0.5} \tag{6}$$

where β is nominally assigned to be unity. This formulation is analogous to the generalization of the velocity scale in the free-convection case (Godfrey and Beljaars 1991) where V_{sm} represents convective boundary-layer scale motions.

4.2 Turbulence Quantities

The turbulence will be represented by σ_w, the standard deviation of the vertical velocity fluctuations for the time-scale range of 0–5 s. The horizontal velocity fluctuations are more contaminated by non-turbulent motions. The vertical velocity fluctuations are more closely related to the mean speed than the mean shear (compare Fig. 2a and b), possibly because of the greater vulnerability of the shear to various errors. However, for near-calm winds (lower left corners of Fig. 2a, b; $V < 0.5\,\mathrm{m\,s^{-1}}$), σ_w is poorly predicted by the mean wind or the mean shear. The generalized velocity scale (Eq. 6) modestly improves the prediction of σ_w for near-calm conditions in that it narrows the cloud of points for the weakest wind conditions. Compare the lower left corners of Fig. 2b and c. The value of σ_w asymptotically vanishes for non-zero generalized velocity scale (Fig. 2c). The standard deviation of the vertical velocity fluctuations for the time scale range of 5–60 s (not shown) depends on the velocity scales in a similar manner.

Non-dimensional turbulence quantities include z/L for both the 0–5 s fluctuations and 5–60 s fluctuations. Unlike the traditional use of z/L as a stability parameter, here we examine the behaviour of z/L as a characteristic of the fluctuating motions and instead define stability in terms of the mean flow (Fr). The turbulence characteristics will also be expressed in terms of correlations between w' and ϕ', and the skewness and kurtosis of the fluxes, where ϕ is potential temperature or one of the horizontal velocity components. We will evaluate the velocity aspect ratio (anisotropy parameter) as

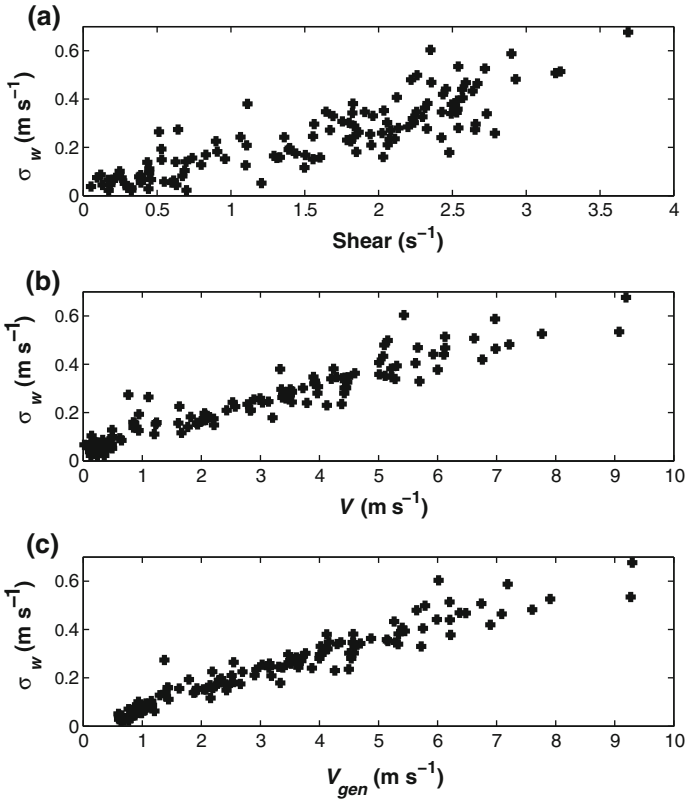

Fig. 2 The dependence of 0–5 s $\sigma_w\,(\mathrm{m\,s^{-1}})$ on: **a** the 1–10 m wind shear $(\mathrm{m\,s^{-1}})$, **b** the wind speed and **c** the generalized velocity scale, $V_{\mathrm{gen}}\,(\mathrm{m\,s^{-1}})$. All quantities are computed from 6-h averages

$$VAR \equiv \frac{\sqrt{2}\sigma_w}{\left(\sigma_u^2+\sigma_v^2\right)^{0.5}}, \tag{7}$$

which becomes unity when all three variances become equal. The ratio of the available potential energy to the kinetic energy increases with stability and increases with scale (Winters et al. 1995; Zilitinkevich et al. 2009). The ratio of the perturbation potential energy to the vertical component of the kinetic energy

$$PE/KE_z \equiv \frac{[T'T']g}{[\theta][w'w'][\partial\theta/\partial z]} \tag{8}$$

where PE refers to the potential energy and KE_z refers to the vertical component of the kinetic energy. This ratio is more sensitive to the stability and scale than the ratio of potential energy to the total kinetic energy since the horizontal velocity fluctuations contain a large non-turbulent contribution.

A measure of relative variability

$$R_{\mathrm{var}} \equiv \frac{[\overline{\phi}^{\,2}]}{[\phi]^2} \tag{9}$$

is computed as the variance of the 1-min averaged fluxes due to the 0–5 or 5–60 s range of scales, divided by the flux averaged over the entire 6-h period where, here, ϕ is the deviation of the 1-min average from the 6-h average. R_{var} will be evaluated for ϕ equal to the heat flux or momentum flux. Large values of R_{var} identify situations where the intermittency is sufficiently large that the interpretation of the 6-h averaged flux is uncertain.

5 Scale and Stability Dependence of Turbulence Characteristics

Both the wind speed and the Froude number can be used to classify the flow characteristics. Although Fr depends on $\delta\theta$ in addition to wind speed, it is generally well correlated with wind speed (Fig. 3a) because $\delta\theta$ is inversely related to wind speed (Fig. 3b). Twenty seven of the 30 6-h records with $Fr < 1$ satisfy the near-calm condition of $V < 0.5\,\text{m}\,\text{s}^{-1}$ while three records are characterized by $0.5\,\text{m}\,\text{s}^{-1} < V < 1.0\,\text{m}\,\text{s}^{-1}$. Coincidentally, the near-calm condition of $V < 0.5\,\text{m}\,\text{s}^{-1}$ also yields 30 6-h records of which 27 correspond to $Fr < 1$. The strongly stable cases and the near-calm cases generally coincide.

We now examine the variation of turbulence characteristics for the entire range of the Froude number, with emphasis on very stable conditions where the Froude number is less than unity. For weaker stability ($Fr > 1$), z/L based on both the 0–5 and 5–60 s range of scales decreases with decreasing stability (increasing Fr, Fig. 4a). The similarity between scale ranges for $Fr > 1$ is probably due to the dominance of both scale ranges by fully developed turbulence. For the most stable regime ($Fr < 1$), the dependence of z/L on Fr shows much more scatter as the turbulence is more related smaller-scale motions compared to the mean flow.

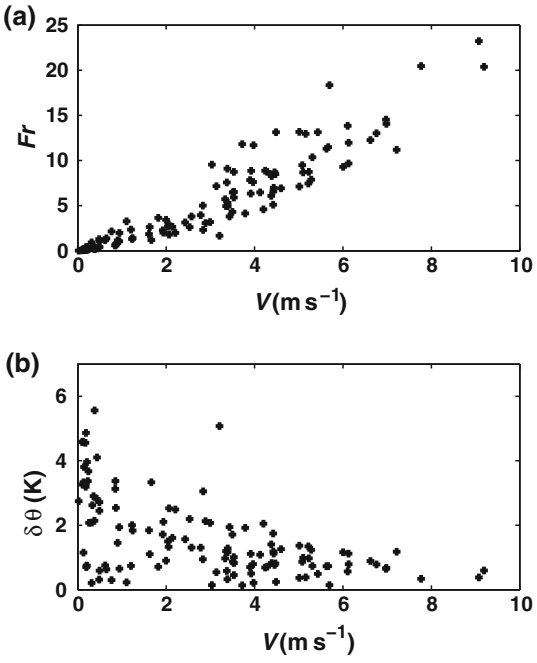

Fig. 3 **a** The dependence of Fr on the 2-m wind speed $V\,(\text{m}\,\text{s}^{-1})$. **b** The dependence of the vertical difference of potential temperature (K) between 1 and 10 m on the 2-m wind speed $(\text{m}\,\text{s}^{-1})$. All quantities are computed from 6-h averages

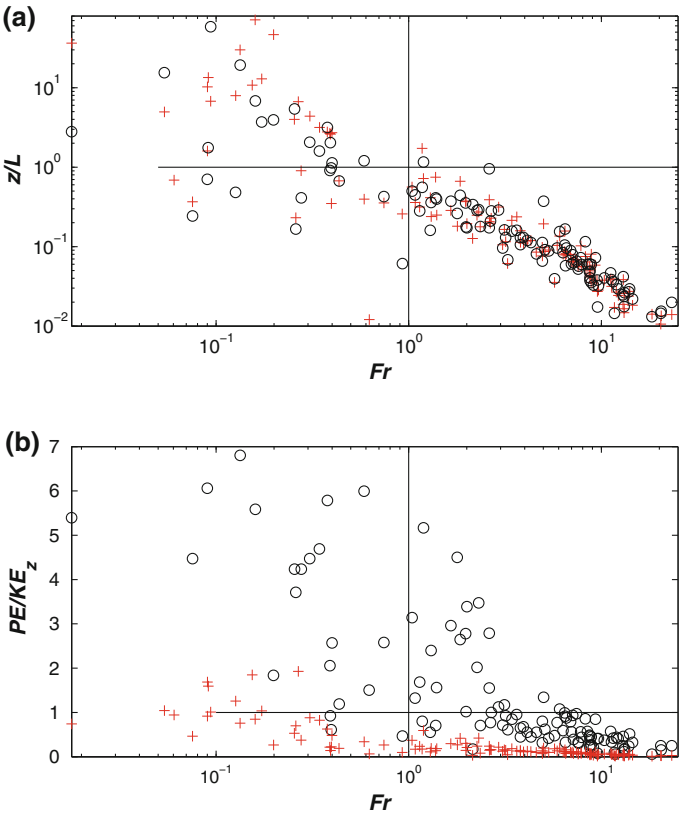

Fig. 4 **a** The dependence of z/L on Fr for the 0–5 s motions (*red plus*) and for the 5–60 s motions (*black circle*). The three 6-h records with very weak upward heat flux are offscale. **b** Ratio of the perturbation potential energy to the vertical kinetic energy (PE/KE_z) as a function of Fr for the 0–5 s motions (*red plus*) and for the 5–60 s motions (*black circle*). For $Fr < 1$, eight of the records for the 5–60 s motions correspond to a ratio greater than 7 and are thus offscale. The thin vertical lines indicate $Fr = 1$ while the *horizontal lines* indicate z/L or $PE/KE_z = 1$. All quantities are computed from 6-h averages

For strong stability ($Fr < 1$), z/L is sometimes $\gg 1$, corresponding to values of L significantly less than 2 m. If L is a useful measure of the dominant eddy size, which is a weaker assumption than the validity of Monin–Obukhov similarity theory, then large values of $z/L \gg 1$ imply that the dominant eddy size is smaller than the 2-m height above ground. This suggests that the eddies at 2 m are sufficiently constrained by the stratification that they are not directly interacting with the ground surface. This is a statistical statement and isolated mixing events interact directly with the surface as well as extend to higher levels.

The ratio of the perturbation potential energy to the vertical component of the kinetic energy (PE/KE_z) for the 0–5 s scale range is much less than one for weaker stability ($Fr > 1$), but increases to order of unity for the strongest stability cases ($F = O(0.1)$, Fig. 4b, red plus). The ratio of potential energy to vertical kinetic energy is much greater for the 5–60 s range of scales. Compared to the 0–5 s motions, the 5–60 s motions are characterized by weaker vertical velocity fluctuations and larger temperature fluctuations for the entire range of stability. PE/KE_z effectively reveals the scale dependence of the fluctuating flow as a function of stability.

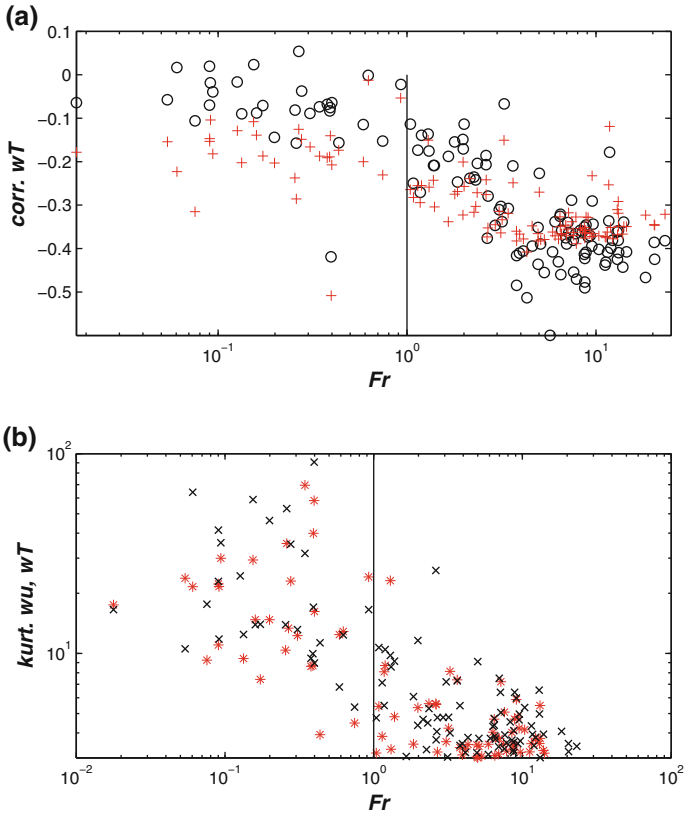

Fig. 5 **a** The correlation between the vertical velocity fluctuations and temperature fluctuations for the 0–5 s motions (*red plus*) and for the 5–60 s motions (*black circle*), as a function of Fr, **b** Kurtosis of the 0–5 s momentum flux (*black cross*) and heat flux (*red plus*). All the quantities are computed from 6-h averages

The large temperature fluctuations associated with weak vertical velocity fluctuations on 5–60 s scales could be related to the longer duration of larger-scale vertical velocity fluctuations. For example, the temperature fluctuations could be posed as $\theta' \sim w'(\mathrm{d}[\theta]/\mathrm{d}z)\tau$, where τ is the time scale of the vertical velocity fluctuations and the primes temporarily represent typical magnitudes of the fluctuating quantities. Since the vertical velocity fluctuations decrease more slowly than linearly with increasing time scale (not shown), this scaling argument predicts increasing θ' with increasing time scale.

The magnitude of the correlation between the 0–5 s vertical velocity fluctuations and temperature fluctuations (Fig. 5a, red plus) is typically about 0.35 for very weak stability ($Fr > 5$). The magnitude of the correlations decreases with increasing stability. For strong stability ($Fr < 1$), the correlation averages only about 0.2 for the 0–5 s scale range. Since turbulence is normally associated with larger correlations, even the 0–5 s scales may be significantly influenced by nonturbulent motions. The magnitude of the correlation for the 5–60 s range of scales averages less than 0.1 for strong stability (Fig. 5a, black circle, $Fr < 1$) such that the transporting motions are a minor part of the fluctuating flow. The correlation coefficients between vertical velocity and along-wind velocity fluctuations (not shown) average only about half of the correlations between vertical velocity and temperature fluctuations.

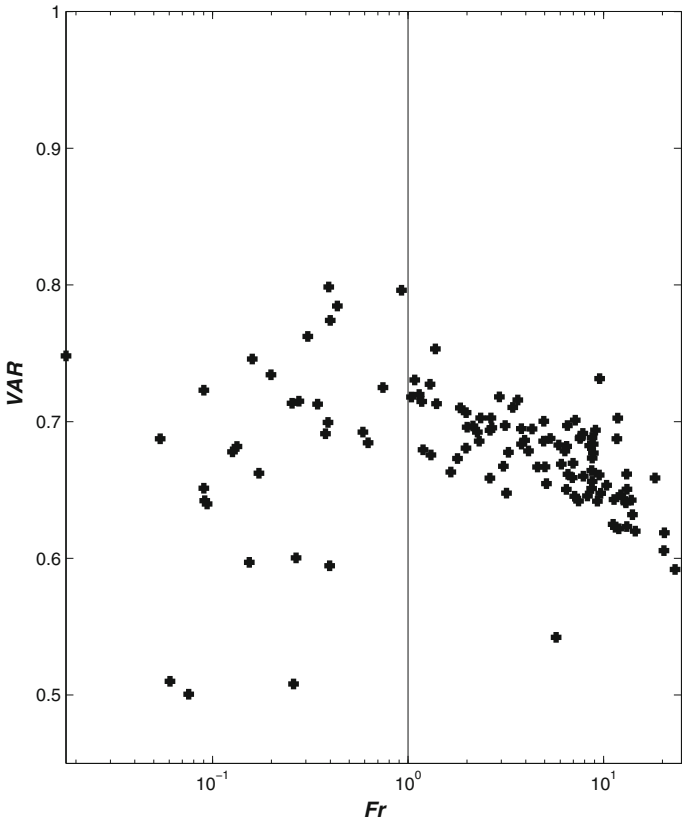

Fig. 6 The 0–5 s $VAR \equiv \sqrt{2}\sigma_w/(\sigma_u^2 + \sigma_v^2)^{0.5}$ as a function of Fr. All the quantities are computed from 6-h averages

The values of the correlations show little relationship to the exact value of Fr for the most stable conditions since the turbulence is no longer closely related to the mean flow.

For weaker stability ($Fr > 1$), the standard deviation of the 1-min fluxes for the 0–5 s range, divided by the 6-h average of this flux (Eq. 9), is typically small compared to unity (not shown). For stronger stability, this ratio is often large compared to unity. This underscores the large within-record variability for very stable conditions due to the influence of isolated mixing events on the record-averaged flux. The kurtosis is often used as a measure of the intermittency of the turbulence (Vindel et al. 2008). The kurtosis of the heat and the momentum fluxes is greater than 10 for most of the very stable records ($Fr < 1$) and approaches 100 for some of the records where one or two events dominate the 6-h flux (Fig. 5b). In contrast, with intermittency typically reported in the literature for the stable boundary layer (Katul et al. 1994), the kurtosis of the heat flux is less than 10. The kurtosis of the heat and momentum fluxes is even larger for the 5–60 s range of scales (not shown). The large variability of the fluxes is an important characteristic of the fluxes for very stable conditions.

The velocity aspect ratio ($\sqrt{2}\sigma_w/(\sigma_u^2 + \sigma_v^2)^{0.5}$) for the 0–5 s motions (Fig. 6) reaches a maximum of about 0.7 for $Fr \approx 1$. The velocity aspect ratio decreases with decreasing stability as Fr becomes large compared to unity. For less stable conditions, the horizontal variance may be dominated by larger eddies that are more constrained by the ground surface

(Mauritsen and Svensson 2007). For the most stable conditions ($Fr < 1.0$), the velocity aspect ratio is characterized by large scatter, but can be significantly smaller than 0.7, evidently because of the strong constraint of the stratification on the vertical motions. Even at only 2-m height, the strong stratification may be more constraining than the ground surface. This dominating impact of stratification on eddy size is consistent with those values of L that are significantly smaller than 2 m for $Fr < 1.0$ (Fig. 4a). As an aside, Zilitinkevich et al. (2009) suggest that large scatter in the velocity aspect ratio for strong stability could result from the wave contribution to the vertical velocity fluctuations, although the wave influence is expected to be small for the 0–5 s range of time scales.

The scatter can be reduced by imposing conditions on non-stationarity across the 6-h records. However, one of the purposes of this investigation is to quantify the large variability of the turbulence between very stable records. The large variability for the very stable regime can be related to the event nature of the flux, and is examined in the next section.

6 Near-Calm Regime

The near-calm regime consists of the thirty 6-h records where the speed of the 6-h vector-average wind is less than $0.5\,\mathrm{m\,s^{-1}}$. While the Froude number and 6-h wind are both useful for contrasting the near-calm regime with stronger winds, they are not useful for predicting the variation of turbulence quantities within the near-calm regime. Inclusion of the submeso velocity (Eq. 5) scale provides only modest improvement for predicting the 6-h turbulence quantities. With current understanding, it is not possible to identify the primary length and velocity scales, if they exist. We proceed with analysis of dimensional variables without scaling.

Since the 6-h averaged turbulent quantities for the near-calm regime are poorly related to the mean 6-h averaged speed and stratification, we now evaluate inter-variable relationships

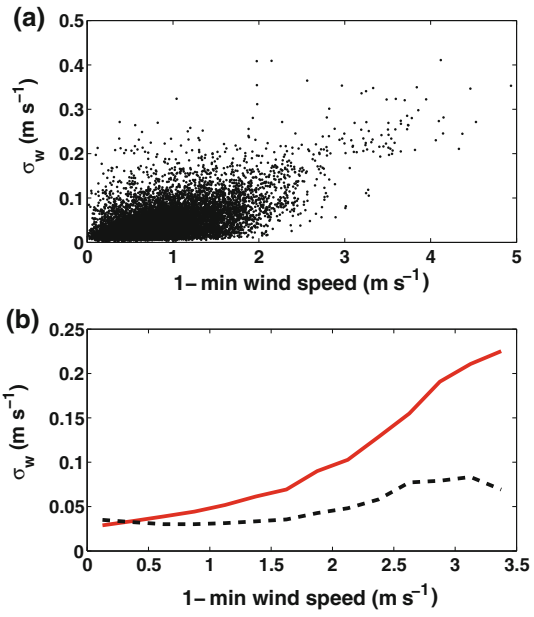

Fig. 7 **a** The dependence of the 1-min $\sigma_w\,(\mathrm{m\,s^{-1}})$ for the 0–5 s fluctuations on the 1-min wind speed. The cloud of points in the lower left part of **a** contains approximately 99% of the points. **b** The dependence of the bin-averaged σ_w on the 1-min wind speed for the 0–5 s fluctuations (*red*) and the 5–60 s fluctuations (*black dashed*)

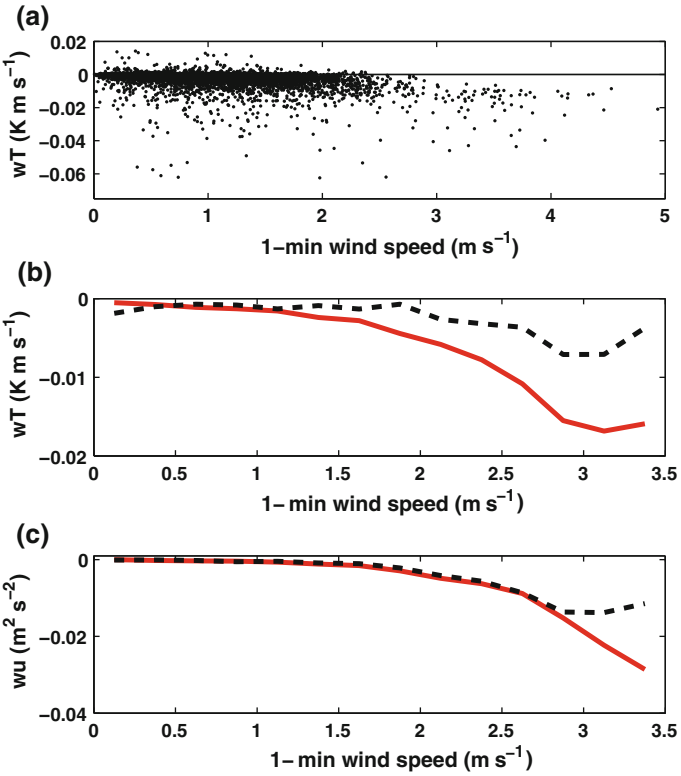

Fig. 8 **a** The dependence of the 1-min averaged 0–5 s heat flux (K m s^{-1}) on the 1-min wind speed (m s^{-1}), **b** corresponding bin-averaged heat flux for the 0–5 s fluctuations (*red solid*) and 5–60 s fluctuations (*black dashed*) and **c** corresponding bin-averaged along-wind momentum flux (m^2 s^{-2}) for the 0–5 s fluctuations (*red solid*) and 5–60 s fluctuations (*black dashed*)

between the 1-min averaged fluxes and the 1-min averaged wind speed and stratification. The 1-min averaged wind and stratification resolves the wave-like modes and other small-scale motions. To examine the influence of these motions on the turbulence, all 1-min periods from the near-calm 6-h records are combined into one dataset containing approximately ten thousand 1-min values. On average, the 1-min values of σ_w tend to increase significantly when the 1-min averaged wind speed exceeds about 1.5 m s^{-1} (Fig. 7), although the scatter is large. A few mixing events occur for weaker wind speeds (Fig. 7a), but account for a very small fraction of the very large number of weaker-wind cases.

On average, the 1-min heat flux (Fig. 8) increases significantly when the wind speed exceeds about 2 m s^{-1}. Heat flux events for speeds less than 1.5 m s^{-1} are infrequent since the cloud of points contain almost 10,000 1-min periods. Consequently, the temporary increases of wind speed to values greater than 2 m s^{-1} substantially increases the probability of generation of turbulence events and significant flux. For speeds less than 1.5 m s^{-1}, the shear is evidentally inadequate to generate significant turbulence, although the remaining very weak turbulence never vanishes. One-min averages of the 0–5 s momentum fluxes (Fig. 8c) exhibit similar dependencies on wind speed compared to that for heat. However, the 5–60 s scales transport as much momentum as the 0–5 s scales, corresponding to a shift of momentum flux to larger time scales compared to the heat flux. The scatter in Figs. 7 and 8 is probably related

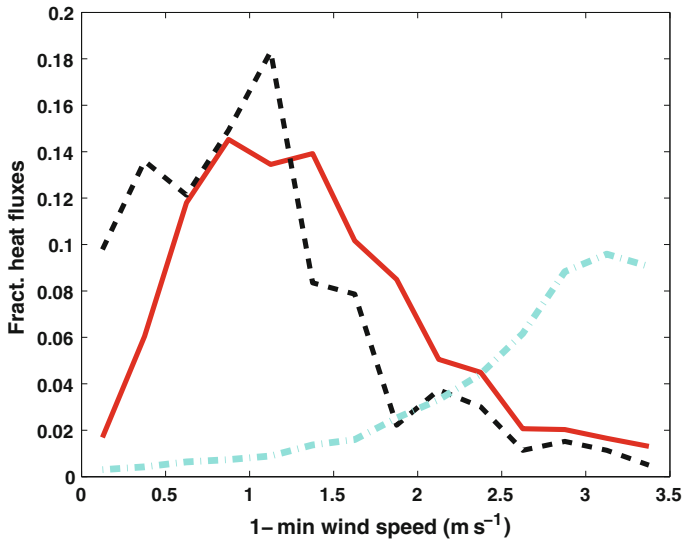

Fig. 9 The dependence of the fraction of the total heat flux for all of the records ($F_{\rm cond}$, K m s^{-1}) on the 1-min wind speed (m s^{-1}) for 1-min averages of the 0–5 s heat flux (K m s^{-1}, *red solid*) and the 5–60 s heat flux (K m s^{-1}, *black dashed*). The relative fractional heat flux ($RF_{\rm cond}/100$, K m s^{-1}) is shown for the 0–5 s range of scales (*cyan*, *dashed dot*)

to the imperfect relationship between the wind speed, shear and wind-profile curvature and failure of the turbulence to completely adjust to the constantly changing wind field.

The more significant winds associated with the mixing events could be a result of the downward mixing of momentum and not a cause of the mixing events. However, there is no systematic lag of the wind speed with respect to the momentum flux, suggesting that downward mixing is not the primary cause of the transient increases in wind speed.

To further study the dependence of the heat flux on wind speed, we define the fractional flux as the total summed contribution from a given wind-speed interval, divided by the total summed flux for the entire near-calm dataset

$$F_{\rm cond} \equiv \frac{(\Sigma w'\theta')_{\rm cond}}{\Sigma w'\theta'}. \tag{10}$$

Here, the sum is carried out over all of the 1-min periods in the near-calm dataset and 'cond' refers to the selection of 1-min periods from a given wind-speed interval. The fractional contribution to the heat flux is greatest for wind speeds of about 1 m s^{-1} for both the 0–5 s range of scales (red line in Fig. 9) and the 5–60 s range of scales (black dashed line in Fig. 9). One-min speeds less than 1 m s^{-1} are more common, but are characterized by very weak heat flux. Speeds greater than 1.5 m s^{-1} are characterized by larger heat flux, but are much less frequent. For comparison, the relative frequency maximum of the 1-min speed occurs at about 0.8 m s^{-1}.

At the same time, the infrequent higher-speed events explain a disproportional fraction of the flux. This can be documented in terms of the relative fractional flux, defined as

$$RF_{\rm cond} \equiv \frac{F_{\rm cond}}{N_{\rm cond}} \tag{11}$$

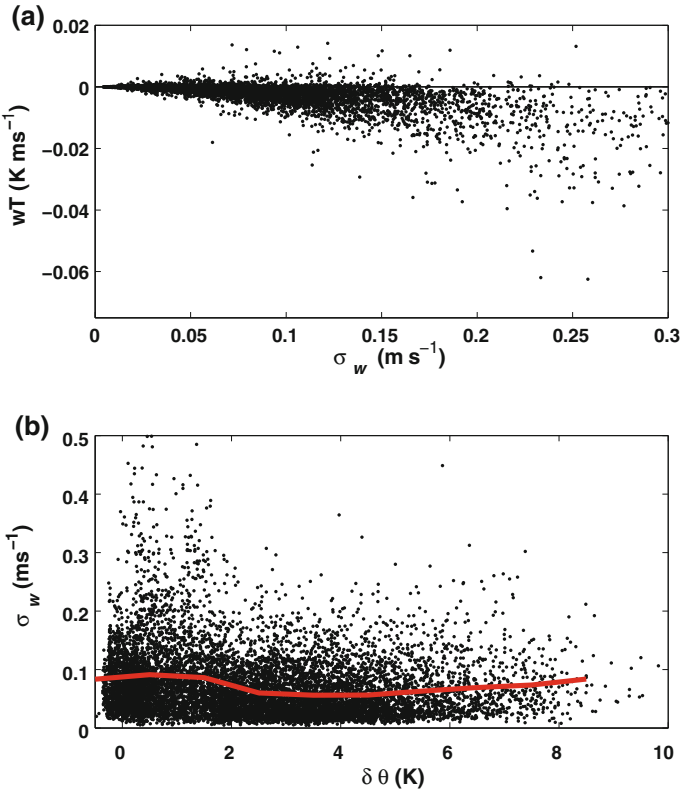

Fig. 10 **a** The dependence of the 1-min averaged 0–5 s heat flux on $\sigma_w\,(\mathrm{m\,s^{-1}})$. **b** The dependence of the 1-min averaged 0–5 s σ_w on $\delta\theta$. The *red line* represents bin-averaged quantities

where N_{cond} is the fraction of 1-min periods occurring within a given wind-speed interval where values of the ratio greater than unity indicate higher than average flux. The relative fractional flux reaches a maximum of 10 at the 1-min speed interval centered at $3.25\,\mathrm{m\,s^{-1}}$ and decreases to values much less than one for the weakest winds. The leveling off of RF_{cond} at the highest winds speeds could be a result of a rapidly decreasing sample size at stronger wind speeds. The distribution of the heat flux is not bimodal because the isolated mixing events have a broad distribution of strength, as also found by Nakamura and Mahrt (2005) for the CASES-99 data. Presumably some of the mixing events are captured in the decay stage or only the edge of the event is captured.

The magnitude of the downward heat flux increases faster than linearly with increasing σ_w, although the scatter is large (Fig. 10a). The maximum downward heat flux seems to be sharply constrained by the value of σ_w. This observation can be interpreted in terms of a maximum downward heat flux that can be supported by a given strength of the turbulence. Bin-averaged values of σ_w show little systematic dependence on the stratification (red line in Fig. 10b). The cases of weakest stratification ($\delta\theta < 3\,\mathrm{K}$) include a few 1-min periods with the strongest turbulence, although these limited number of cases have only a small influence on the bin-averaged heat flux and occur almost exclusively with stronger winds. The ratio σ_w/V (not shown) also shows little systematic dependence on $\delta\theta$. The generation of mixing events depends mainly on the wind speed.

7 Conclusions

Nocturnal sonic anemometer measurements at 2 m were analyzed to examine the turbulence mixing in very weak winds. The Froude number (as defined by Eq. 4) was found to be a better posed stability function than the Richardson number for very strong stratification since the Richardson number can reach extremely large values for very weak winds. One of the goals of this study was to examine the relationship (or lack of) between the turbulence and the mean wind and temperature fields. Therefore, z/L is not used as an external stability parameter, but is used instead as a characteristic of the turbulence. Because of the strong influence of infrequent mixing events for near-calm winds, a long 6-h averaging time was used. Even then, the averaged flux for very stable conditions can be dominated by a limited number of events associated with flow acceleration. The large within-record and between-record variability of the flux is an important characteristic of the turbulence for very stable conditions.

As the stability increases (decreasing Froude number), z/L increases and the correlations of w' with θ', u' and v', all decrease. The ratio of the vertical velocity fluctuations to the horizontal velocity fluctuations, $\sqrt{2}\sigma_w/(\sigma_u^2+\sigma_v^2)^{0.5}$, decreases with decreasing stability and increasing wind speed, presumably because increasingly larger eddies are more constrained by the ground surface. This ratio also decreases for the very stable conditions when the strong stratification severely inhibits vertical motions and L can be significantly smaller than the 2-m height above ground. This inference is visualized by videos of machine-generated fog (http://www.youtube.com/watch?v=8fu1bvGIF44).

The ratio of the available potential energy to the vertical component of the kinetic energy increases significantly with increasing stability. This energy ratio increases substantially with scale, serving as an effective representation of the change of scale dependence with stability.

For very stable conditions ($Fr < 1$), the relationship between the turbulence and the mean flow becomes more uncertain, partly due to event-like shear generation of turbulence by non-stationary submeso motions and associated large skewness and kurtosis of the turbulence quantities. Complete separation between the turbulence and non-turbulent motions becomes problematic for very stable conditions and the characteristics of the fluctuating flow change only gradually with increasing time scale.

Very stable conditions ($Fr < 1$) generally correspond to the vector-averaged wind speed $< 0.5\,\mathrm{m\,s^{-1}}$. Such winds are referred to as the near-calm wind regime, which also occurs for a few cases with weak stratification. In this regime, the behaviour of the turbulence is no longer related to the mean wind speed or stratification. The turbulence events in the near-calm regime are much more likely to occur when the 1-min wind speed temporarily exceeds about $2.0\,\mathrm{m\,s^{-1}}$. Significant scatter is probably due to non-stationarity, complex vertical wind profiles and failure of the turbulence to achieve equilibrium with the changing wind profiles. Except for very weak stratification when σ_w is larger, the turbulent flux and σ_w are not systematically related to transient variations of the stratification.

For near-calm winds, the correlation between the vertical velocity and temperature fluctuations on time scales of 0–5 s averages is only about 0.2, suggesting that non-turbulent motions influence even these small scales. The fluctuations on scales of 5–60 s lead to even weaker correlations and a more erratic flux, although after extensive averaging, this heat flux is downwards. The motions on scales of 5–60 s are characterized by very weak vertical velocity fluctuations, which are only weakly correlated to the temperature fluctuations. However, the temperature fluctuations are large on these scales, leading to significant heat flux in spite of weak correlations. Present physical understanding of the near-calm case is insufficient to determine the primary governing length and velocity scales required for similarity theory. A more detailed analysis of the evolution of mixing events and their dynamics is required.

Acknowledgments The author gratefully acknowledges important comments from Christoph Thomas, Dean Vickers and Andrey Grachev. The FLOSSII and CASES-99 data were provided by the Integrated Surface Flux Facility of the National Center for Atmospheric Research. This material is based upon work supported by NSF Grant ATM-0607842 and ARO Contract W911FN05C0067.

References

Acevedo O, Mahrt L (2010) Systematic vertical variation of mesoscale fluxes in the stable boundary layer. Boundary-Layer Meteorol 135:19–30

Baas P, Steeneveld G, van de Weil B, Holtslag A (2006) Exploring self-correlation in the flux–gradient relationships for stably stratified conditions. J Atmos Sci 63:3045–3054

Balsley B, Svensson G, Tjernström M (2008) On the scale-dependence of the gradient Richardson number in the residual layer. Boundary-Layer Meteorol 127:57–72

Basu S, Porté-Agel F, Foufoula-Georgiou E, Vinuesa JF, Pahlow M (2006) Revisiting the local scaling hypothesis in stably stratified atmospheric boundary-layer turbulence: an integration of field and laboratory measurements with large-eddy simulations. Boundary-Layer Meteorol 119:473–500

Belušić D, Güttler I (2010) Can mesoscale models reproduce meandering motions?. Q J Roy Meteorol Soc 136:553–565

Bodine D, Klein P, Arms S, Shapiro A (2009) Variability of surface air temperature over gently sloped terrain. J Appl Meteorol 48:1117–1141

Bou-Zeid E, Higgins C, Huwald H, Meneveau C, Parlange M (2010) Field study of the dynamics and modelling of subgrid scale turbulence in a stable atmospheric surface layer over a glacier. J Fluid Mech 64:216–227

Cuxart J, Jiménez M, Martínez D (2007) Nocturnal mesobeta basin and katabatic flows on a midlatitude island. Mon Weather Rev 135:918–932

Derbyshire S (1999) Boundary-layer decoupling over cold surfaces as a physical boundary-instability. Boundary-Layer Meteorol 90:297–325

Desjardins R, MacPherson J, Schuepp P, Karanja F (1989) An evaluation of aircraft flux measurements of CO_2, water vapor and sensible heat. Boundary-Layer Meteorol 47:55–69

Finnigan J (1999) A note on wave–turbulence interaction and the possibility of scaling the very stable boundary layer. Boundary-Layer Meteorol 90:529–539

Finnigan J, Einaudi F, Fua D (1984) The interaction between an internal gravity wave and turbulence in the stably-stratified nocturnal boundary layer. J Atmos Sci 41:2409–2436

Friehe C, Shaw W, Rogers D, Davidson K, Large W, Stage S, Crescenti G, Khalsa S, Greenhut G, Li F (1991) Air–sea fluxes and surface layer turbulence around a sea-surface temperature front. J Geophys Res 96:8593–8609

Fritts D, Wang L, Werne J, Lund T, Wan K (2009) Gravity wave instability dynamics at high reynolds numbers, part II: turbulence evolution, structure, and anisotropy. J Atmos Sci 66:1149–1171

Galperin B, Sukoriansky S (2010) Geophysical flows with anisotropic turbulence and dispersive waves: flows with stable stratification. Atmos Sci Lett 8:65–84

Galperin B, Sukoriansky S, Anderson P (2007) On the critical Richardson number in stably stratified turbulence. Atmos Sci Lett 8:65–69

Godfrey J, Beljaars A (1991) On the turbulent fluxes of buoyancy, heat and moisture at the air–sea interface at low wind speeds. J Geophys Res 96:22043–22048

Grachev A, Fairall C, Persson P, Andreas E, Guest P (2005) Stable boundary-layer scaling regimes: the SHEBA data. Boundary-Layer Meteorol 116:201–235

Heywood G (1933) Katabatic winds in a valley. Q J Roy Meteorol Soc 59:43–57

Hicks B (1981) An examination of turbulence statistics in the surface boundary layer. Boundary-Layer Meteorol 21:389–402

Howell J, Sun J (1999) Surface layer fluxes in stable conditions. Boundary-Layer Meteorol 90:495–520

Katul G, Albertson J, Parlange M, Chu CR, Stricker H (1994) Conditional sampling, bursting and the intermittent structure of sensible heat flux. J Geophys Res 99:22869–22876

Klipp C, Mahrt L (2003) Conditional analysis of an internal boundary layer. Boundary-Layer Meteorol 108: 1–17

Mahrt L (2007) Weak-wind mesoscale meandering in the nocturnal boundary layer. Environ Fluid Mech 7:331–347
Mahrt L (2008) The influence of transient flow distortion on turbulence in stable weak-wind conditions. Boundary-Layer Meteorol 127:1–16
Mahrt L (2009) Characteristics of submeso winds in the stable boundary layer. Boundary-Layer Meteorol 130:1–14
Mahrt L, Vickers D (2006) Extremely weak mixing in stable conditions. Boundary-Layer Meteorol 119:19–39
Mahrt L, Richardson S, Seaman N, Stauffer D (2010) Nonstationary drainage flows and motions in the cold pool. Tellus 62A:698–705
Mauritsen T, Svensson G (2007) Observations of stably stratified shear-driven atmospheric turbulence at low and high Richardson numbers. J Atmos Sci 64:645–655
Meillier Y, Frehlich RG, Jones RM, Balsley BB (2008) Modulation of small-scale turbulence by ducted gravity waves in the nocturnal boundary layer. J Atmos Sci 65:1414–1427
Nakamura R, Mahrt L (2005) A study of intermittent turbulence with CASES-99 tower measurements. Boundary-Layer Meteorol 114:367–387
Nappo C, Chimonas G (1992) Wave exchange between the ground surface and a boundary-layer critical level. J Atmos Sci 49:1075–1091
Nappo CJ, Miller DR, Hiscox AL (2008) Wave-modified flux and plume dispersion in the stable boundary layer. Boundary-Layer Meteorol 129:211–223
Smedman AS (1988) Observations of a multi-level turbulence structure in a very stable atmospheric boundary layer. Boundary-Layer Meteorol 44:231–253
Sorbjan Z (2010) Gradient-based scales and similarity laws in the stable boundary layer. Q J Roy Meteorol Soc 136:1243–1254
Sun J, Lenschow DH, Burns SP, Banta RM, Newsom RK, Coulter R, Frasier S, Ince T, Nappo C, Balsley B, Jensen M, Mahrt L, Miller D, Skelly B (2004) Atmospheric disturbances that generate intermittent turbulence in nocturnal boundary layers. Boundary-Layer Meteorol 110:255–279
Tjernström M, Balsley BB, Svensson G, Nappo C (2009) The effects of critical layers on residual layer turbulence. J Atmos Sci 66:468–480
Van de Wiel BJH, Moene A, Hartogenesis G, Bruin HD, Holtslag AAM (2003) Intermittent turbulence in the stable boundary layer over land, part III: a classification for observations during CASES-99. J Atmos Sci 60:2509–2522
Viana S, Yagüe C, Maqueda G (2009) Propagation and effects of a mesoscale gravity-wave over a weakly-stratified stable boundary layer during SABLES2006 field campaign. Boundary-Layer Meteorol 133:165–188
Viana S, Terradellas S, Yagüe C (2010) Analysis of gravity waves generated at the top of a drainage flow. J Atmos Sci 67:3949–3966
Vindel J, Yagüe C, Redondo J (2008) Structure function analysis and intermittency in the atmospheric boundary layer. Nonlinear Process Geophys 15:915–929
Vosper S, Brown A (2008) Numerical simulations of sheltering in valleys: the formation of nighttime cold-air pools. Boundary-Layer Meteorol 127:429–448
Whiteman C (2000) Mountain meteorology. Oxford University Press, New York
Winters K, Lombard P, Riley J, D'Asaro E (1995) Available potential energy and mixing in density-stratified fluids. J Fluid Mech 289:115–128
Yagüe C, Viana S, Maqueda G, Redondo J (2006) Influence of stability on the flux–profile relationships for wind speed, ϕ_m and temperature, ϕ_h, for the stable atmospheric boundary layer. Nonlinear Process Geophys 13:185–203
Yao W, Zhong S (2009) Nocturnal temperature inversions in a small, enclosed basin and their relationship to ambient atmospheric conditions. Meteorol Atmos Phys 103:195–210
Zilitinkevich S, Elperin T, Kleeorin N, Rogachevskii I (2007) Energy-and flux-budget (EFB) turbulence closure model for stably stratified flows, part I: steady state homogeneous regimes. Boundary-Layer Meteorol 125:167–191
Zilitinkevich S, Elperin T, Kleeorin N, L'vov V, Rogachevskii I (2009) Energy- and flux-budget turbulence closure model for stably stratified flows, part II: the role of internal gravity waves. Boundary-Layer Meteorol 133:139–164